

RESEARCH ARTICLE

Novel salicyloylhydrazone derivatives and corresponding terbium(III) complexes: Synthesis and properties research

 Rong Xiao^{1,2} | Wei Huang³ | Xiaoming Xiao² | Yanhong Liu³ | Dongcai Guo³ 
¹College of Educational science, Hunan Normal University, Changsha, China

²College of Chemistry and Chemical Engineering, Hunan Normal University, Changsha, China

³College of Chemistry and Chemical Engineering, Hunan University, Changsha, China
Correspondence
 Xiaoming Xiao, College of Chemistry and Chemical Engineering, Hunan Normal University, Changsha 410081, China.
 Email: xmxiao@hunnu.edu.cn

 Dongcai Guo, College of Chemistry and Chemical Engineering, Hunan University, Changsha 410082, China.
 Email: dcguo2001@hnu.edu.cn
Funding information

Changsha Science and Technology Bureau, Grant/Award Numbers: kq1701029 and kq1701164; Hunan Provincial Science and Technology Department, Grant/Award Number: 2016SK2064; Innovative Research Team in University, Grant/Award Number: IRT1238; Instrument sharing platform of Hunan university; National Natural Science Foundation of China, Grant/Award Numbers: 21341010, J1210040 and J1103312; Natural Science Foundation of Hunan Province, Grant/Award Number: 11JJ5005; China Outstanding Engineer Training Plan for Students of Chemical Engineering and Technology in Hunan University, Grant/Award Number: MOE-No.2011-40

Abstract

Four novel salicyloylhydrazone derivatives and their terbium(III) complexes were synthesized and characterized. The thermal analysis results showed that the terbium(III) complexes possessed good thermal stability. The fluorescence research results showed that the terbium(III) complex substituted by phenyl possessed the best fluorescence intensity among them, and its fluorescence quantum yield was also the highest. The exploration of the electrochemical properties indicated that the introduction of electron-donating groups to the ligand can increase the highest occupied molecular orbital (HOMO) energy levels and decrease the oxidation potential of the corresponding terbium(III) complexes. The introduction of electron-withdrawing groups to the ligand can reduce their HOMO energy levels and increase their oxidation potential. The results showed that the terbium(III) complexes are good candidates for luminescent material.

KEYWORDS

electrochemical properties, fluorescence, salicyloylhydrazone, synthesis, terbium(III) complexes

1 | INTRODUCTION

The luminescence properties of rare earth complexes have drawn much attention owing to the distinctiveness and diversity of the properties, and the wide range of applications in many fields. Among rare earth ions, terbium(III) ion (Tb^{3+}) has been widely studied. For example, Xin et al. reported a new terbium complex ($Tb(eb-PMP)_3TPPO$) with efficient electroluminescence (EL),^[1] and they also reported the effect of the neutral ligands (TPPO, Phen) on the photoluminescence (PL) and EL properties of the terbium complexes.^[2] Cui et al. reported an effective green phosphorescent organic electroluminescent device with a terbium complex as the sensitizer.^[3] Law et al. reported an

emissive terbium probe for multiphoton *in vitro* cell imaging.^[4] Ye et al. reported a terbium complex-based luminescent probe ($BMTA-Tb^{3+}$) for the recognition and luminescence detection of hydrogen peroxide (H_2O_2) in aqueous solutions.^[5] However, salicyloylhydrazone contains nitrogen and oxygen atoms, and it can coordinate with metal ions. Their derivatives were reported as excellent ligands and as highly selective Schiff base fluorescent chemosensors.^[6,7]

In order to obtain strong luminescent complexes, researchers have designed and synthesized a large number of organic ligands and have tried to explore the effect of different structures or constituent groups on the luminescence properties.^[8,9] However, there also existed some problems, such as poor thermal stability,

weak luminescence intensity, etc. These defects limited their application fields. Through the modification of the ligand, their solubility, thermal stability and luminescent properties can be improved, and their application potential can also be enhanced.^[10,11] Therefore, this method has aroused people's attention, and we also have done some work in this field.

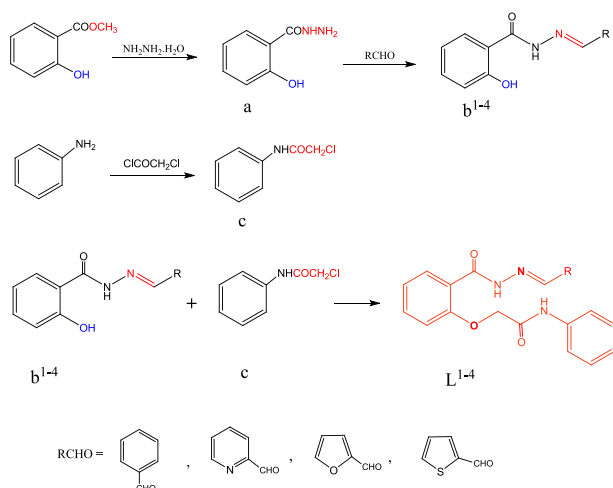
In this article, on the basis of our preceding work, four novel hydroelectrical derivatives were synthesized and characterized by ¹H-NMR, ¹³C-NMR and mass spectrometry (MS). The synthetic routes are shown in Scheme 1. Furthermore, terbium(III) complexes were also prepared, and their structure and composition were explored by molar conductance, elemental analysis, UV spectra, IR spectra and thermal analysis. Moreover, their thermal stability, electrochemical properties and fluorescence properties were also discussed. These complexes will possibly be used as fluorescent paints, and will be explored in our future research work.

2 | EXPERIMENTAL

2.1 | Materials and method

Pyridine-2-formaldehyde (98%), 2-thiophene formaldehyde (98%), Tb₄O₇ (99.99%), formaldehyde, dehydrator, mentalist salivary, thora-zine hydrate and other reagents (analytical reagent grade) were purchased from commercial suppliers.

The ¹H- and ¹³C-NMR spectra were recorded in dimethyl sulfoxide (DMSO)-*d*₆/deuterated chloroform (CDCl₃) on a Bruker spectrometer (400 MHz) with tetramethylsilane (TMS) as an internal standard. MS was measured with a MAT95XP mass spectrometer. Melting points of all compounds were determined on an X-4 binocular microscope. Elemental analysis of the complexes was carried out on a Varietal 111 (Germany) CHNS analyzer. Molar conductance was measured using a DDS-12A conductivity instrument. Ultraviolet-visible (UV-vis) spectra were recorded on a Lab Tech UV-2100 magnetometer, with dimethylformamide (DMF) as solvent and reference. Infrared (IR) spectra (400–4000 cm⁻¹) were obtained



SCHEME 1 The synthetic route for the salicyloylhydrazone derivatives

in potassium bromide discs by a PER KINGMAKER Spectrum One. Thermogravimetric analysis (TGA) was carried out on a NETZSCH STA 409PC thermal gravimetric analyzer. The fluorescence spectra were measured using a HIACHI F-2700 fluorescence magnetometer at room temperature, using powder samples, and both the excitation and emission light slits were 5.0 nm. Cyclic voltmeter curves were tested using three electrodes (a glassy electrode, a platinum electrode and a saturated Camelot electrode), with scenery as external standard, and nitrite solution as the supporting electrolyte and DMSO as the solvent, the test scanning speed was 100 V s⁻¹ and the sensitivity was 1 A.

2.2 | General synthesis procedure of the intermediates

2.2.1 | Synthesis of compound **a**

A mixture of menthyl salicylate (50 mmol, 7.60 g) and absolute alcohol (15 mL) was added to a 250 mL three-necked flask, and then 10 mL of hydrazine hydrate was gradually added drop by drop. The reaction mixture was heated to 80°C and refluxed for 10 h, cooled to room temperature and filtered. The residue was recrystallized from distilled water, and then a white crystal was obtained.^[12] Yield was 87%.

2.2.2 | Synthesis of compound **b**¹⁻⁴

Salicylhydrazide (20 mmol, 3.04 g) was dissolved in 20 mL absolute alcohol in a 250 mL three-necked flask, and then heated. When the temperature was stable at 85°C, benzaldehyde (20 mmol, 2.12 g) was gradually added drop by drop with the reaction lasting for 4 h. Cooled to room temperature and filtered, then washed several times with hot absolute alcohol. The white solid of compound **b**¹ was obtained.^[13,14] The general synthesis procedures of **b**²⁻⁴ were similar to that of **b**¹.

2-Hydroxy-*N'*-benzylidene-2-benzoylhydrazone (**b**¹)

A white solid. Yield: 88%. ¹H-NMR (400 MHz, DMSO-*d*₆) δ 11.84 (s, 2H), 8.47 (s, 1H), 7.90 (d, *J* = 7.7 Hz, 1H), 7.79–7.72 (m, 2H), 7.51–7.42 (m, 4H), 7.01–6.93 (m, 2H); MS (EI) *m/z* (%): 241 (*m* + 1, 3), 240 (*m*, 18), 138 (3), 137 (36), 121 (100), 120 (52), 119 (9), 93 (17), 92 (5), 65 (14).

2-Hydroxy-*N'*-(pyridine-2-methylene)-2-benzoylhydrazone (**b**²)

A light-yellow solid. Yield: 81%. ¹H-NMR (400 MHz, DMSO-*d*₆) δ 12.02 (s, 1H), 11.67 (s, 1H), 8.64 (d, *J* = 4.4 Hz, 1H), 8.48 (s, 1H), 8.00 (d, *J* = 7.9 Hz, 1H), 7.89 (dd, *J* = 19.6, 7.7 Hz, 2H), 7.45 (dd, *J* = 12.9, 5.8 Hz, 2H), 7.02–6.93 (m, 2H); MS (EI) *m/z* (%): 42 (*m* + 1, 5), 241 (*m*, 26), 122 (4), 121 (54), 120 (100), 94 (3), 93 (15), 92 (43), 66 (2), 65 (19).

2-Hydroxy-*N'*-(furan-2-methylene)-2-benzoylhydrazone (**b**³)

A light-yellow solid. Yield: 84%. ¹H-NMR (400 MHz, DMSO-*d*₆) δ 11.82 (s, 1H), 11.79 (s, 1H), 8.35 (s, 1H), 7.91–7.81 (m, 2H), 7.44 (t, *J* = 7.4 Hz, 1H), 6.97 (dd, *J* = 11.2, 7.3 Hz, 3H), 6.66 (s, 1H); MS (EI)

m/z (%): 231 ($m + 1$, 5), 230 (m , 30), 138 (2), 137 (19), 121 (100), 110 (59), 94 (3), 93 (17), 81 (4), 66 (2), 65 (18), 52 (5).

2-Hydroxy-*N'*-(thiophene-2-methylene)-2-benzoylhydrazine (**b⁴**)

A light-yellow solid. Yield: 85%. ¹H-NMR (400 MHz, DMSO-*d*₆) δ 11.81 (s, 2H), 8.67 (s, 1H), 7.85 (d, $J = 7.7$ Hz, 1H), 7.71 (d, $J = 5.0$ Hz, 1H), 7.51 (d, $J = 3.5$ Hz, 1H), 7.44 (t, $J = 7.7$ Hz, 1H), 7.20–7.14 (m, 1H), 6.97 (dd, $J = 12.1, 6.2$ Hz, 2H); MS (EI) m/z (%): 248 ($m + 2$, 1), 247 ($m + 1$, 4), 246 (m , 23), 138 (4), 137 (43), 126 (50), 121 (100), 120 (29), 99 (5), 93 (19), 92 (5), 65 (19).

2.2.3 | Synthesis of compound **c**

Phenylamine (50 mmol, 4.65 g) and ethylic acid (40 mL) was added to a 500 mL beaker, and then chloroacetyl chloride (50 mmol, 5.60 g) was added dropwise under an ice bath. The reaction mixture was stirred for 30 min under an ice bath, and then stirred at room temperature for another 1 h. The reaction mixture was poured into saturated sodium acetate solution (200 mL), and then filtered, washed several times; the residue was recrystallized from the mixed solution of ethanol and water. The compound **c** was obtained.

2.2.4 | Synthesis of the salicyloylhydrazone derivatives **L¹⁻⁴**

Salicylhydrazine benzylidene (2.40 g, 10 mmol) was dissolved in DMF (20 mL) in a 250 mL three-necked flask. Then, some absolute potassium carbonate (K₂CO₃) was added, heated to 80°C and refluxed for 1 h. After that, 10 mL of 2-chloride-*N*-acetyl aniline DMF solution was added drop by drop and a little potassium iodide (KI) was also added, then refluxed for 3 h. Next the mixture was cooled to room temperature and poured into 300 mL of distilled water, after which the solution was neutralized with 2 mol L⁻¹ dilute hydrochloric acid. Subsequently, filtered and washed until the water was neutral. The residue was dried for three days. Then washed three times and recrystallized three times from acetic ether. The white solid compound **L¹** was obtained. The general synthesis procedures of **L²⁻⁴** were similar to that of **L¹**.

2-(2-(2-Benzylidene)carbohydrazide)phenoxy)-*N*-phenylacetamide (**L¹**)

A white powder. Yield: 54%; melting point (m.p.) 158–160°C. ¹H-NMR (400 MHz, DMSO-*d*₆) δ 12.09 (s, 1H), 10.38 (s, 1H), 8.43 (s, 1H), 7.78 (d, $J = 7.6$ Hz, 1H), 7.71 (dd, $J = 12.3, 5.2$ Hz, 4H), 7.56 (t, $J = 7.9$ Hz, 1H), 7.45 (t, $J = 9.3$ Hz, 3H), 7.33 (t, $J = 7.6$ Hz, 2H), 7.23 (d, $J = 8.3$ Hz, 1H), 7.17 (t, $J = 7.5$ Hz, 1H), 7.10 (t, $J = 7.6$ Hz, 1H), 4.98 (s, 2H); ¹³C-NMR (101 MHz, DMSO-*d*₆) δ 167.29, 162.72, 156.04, 148.34, 138.71, 134.68, 133.31, 130.95, 130.67, 129.39 (2C₁), 129.38 (2C₂), 127.61 (2C₃), 124.35, 123.60, 122.27, 119.92 (2C₄), 114.41, 68.40; MS (EI) m/z (%): 373 (m , 3), 271 (5), 270 (25), 254 (30), 253 (10), 252 (2), 227 (6), 226 (28), 178 (4), 177 (6), 151 (9), 150 (14), 134 (27), 121 (100), 106 (56), 93 (48), 92 (10), 77 (20), 65 (13); Anal. Calcd for C₂₂H₁₉N₃O₃: C, 70.76; H, 5.13; N, 11.25. Found: C, 70.41, H, 5.21; N, 11.29.

2-(2-(2-Pyridine-2-methylene)carbohydrazide)phenoxy)-*N*-phenylacetamide (**L²**)

A light-yellow powder. Yield: 45%; m.p. 147–150°C. ¹H-NMR (400 MHz, DMSO-*d*₆) δ 12.30 (s, 1H), 10.38 (s, 1H), 8.64 (d, $J = 4.6$ Hz, 1H), 8.46 (s, 1H), 8.00 (d, $J = 7.9$ Hz, 1H), 7.92 (t, $J = 7.1$ Hz, 1H), 7.81 (dd, $J = 7.6, 1.4$ Hz, 1H), 7.65 (t, $J = 9.5$ Hz, 2H), 7.63 (m, 1H), 7.47 (m, 1H), 7.34 (t, $J = 7.9$ Hz, 2H), 7.23 (t, $J = 7.3$ Hz, 1H), 7.18 (t, $J = 7.5$ Hz, 1H), 7.10 (t, $J = 7.4$ Hz, 1H), 4.99 (s, 2H); ¹³C-NMR (101 MHz, CDCl₃) δ 166.19, 164.63, 156.09, 152.14, 148.05, 139.12, 137.86, 137.57, 133.22, 129.80, 128.76 (3C₁), 126.01, 124.30 (2C₂), 122.25, 120.09 (2C₃), 113.63, 68.13; MS (EI) m/z (%): 376 ($m + 2$, 1), 375 ($m + 1$, 3), 374 (m , 10), 255 (10), 254 (6), 253 (2), 135 (2), 134 (5), 121 (47), 120 (100), 106 (30), 92 (44), 79 (8), 77 (13), 65 (22); Anal. Calcd for C₂₁H₁₈N₄O₃: C, 67.37; H, 4.85; N, 14.96. Found: C, 67.17; H, 4.60; N, 15.16.

2-(2-(2-Furan-2-methylene)carbohydrazide)phenoxy)-*N*-phenylacetamide (**L³**)

A light-yellow powder. Yield: 33%; m.p. 153–155°C. ¹H-NMR (400 MHz, DMSO-*d*₆) δ 12.07 (s, 1H), 10.40 (s, 1H), 8.33 (s, 1H), 7.91 (s, 1H), 7.80 (d, $J = 7.6$ Hz, 1H), 7.70 (d, $J = 8.3$ Hz, 2H), 7.58 (t, $J = 7.9$ Hz, 1H), 7.37 (t, $J = 7.8$ Hz, 2H), 7.25 (d, $J = 8.4$ Hz, 1H), 7.17 (t, $J = 7.5$ Hz, 1H), 7.12 (t, $J = 7.4$ Hz, 1H), 6.96 (d, $J = 3.3$ Hz, 1H), 6.70–6.66 (m, 1H), 4.98 (s, 2H); ¹³C-NMR (101 MHz, CDCl₃) δ 166.44, 163.12, 155.90, 149.40, 144.71, 139.04, 137.76, 133.30, 131.42, 128.86 (3C₁), 124.42, 122.22, 120.20 (2C₂), 113.91, 113.24, 111.91, 68.10; MS (EI) m/z (%): 365 ($m + 2$, 1), 364 ($m + 1$, 4), 363 (m , 13), 271 (3), 270 (14), 254 (34), 253 (6), 252 (1), 226 (29), 134 (15), 121 (100), 106 (59), 93 (29), 92 (8), 79 (5), 77 (16), 65 (10); Anal. Calcd for C₂₀H₁₇N₃O₄: C, 66.11; H, 4.72; N, 11.56. Found: C, 66.21; H, 4.63; N, 11.46.

2-(2-(2-Thiophene-2-methylene)carbohydrazide)phenoxy)-*N*-phenylacetamide (**L⁴**)

A light-yellow powder. Yield: 37%; m.p. 155–157°C. ¹H-NMR (400 MHz, DMSO-*d*₆) δ 12.04 (s, 1H), 10.36 (s, 1H), 8.62 (s, 1H), 7.80 (m, 1H), 7.73 (m, 3H), 7.56 (dd, $J = 11.5, 4.3$ Hz, 1H), 7.43 (d, $J = 3.5$ Hz, 1H), 7.35 (t, $J = 7.8$ Hz, 2H), 7.22 (d, $J = 8.3$ Hz, 1H), 7.19 (m, 2H), 7.11 (t, $J = 7.5$ Hz, 1H), 4.97 (s, 2H); ¹³C-NMR (101 MHz, CDCl₃) δ 166.43, 163.11, 155.87, 144.62, 138.76, 137.86, 133.37, 131.51, 130.93, 129.00, 128.90 (3C₁), 127.45, 124.43, 122.21, 120.17 (2C₂), 113.27, 68.08; MS (EI) m/z (%): 380 ($m + 1$, 2), 379 (m , 4), 271 (5), 270 (31), 254 (30), 253 (11), 252 (3), 227 (7), 226 (40), 178 (3), 177 (7), 151 (9), 150 (15), 134 (23), 121 (100), 106 (53), 93 (32), 92 (9), 79 (5), 77 (14), 65 (9); Anal. Calcd for C₂₀H₁₇N₃O₃S: C, 63.31; H, 4.52; N, 11.07. Found: C, 63.50; H, 4.12; N, 11.01.

2.3 | Synthesis of the terbium(III) complexes

Ligand **L¹** (0.38 g, 1 mmol) was added into absolute alcohol (50 mL) in a 250 mL three-necked flask and heated to 80°C. After being fully dissolved, the terbium nitrate alcohol solution (5 mL) was added and refluxed for 0.5 h. The pH value of the reaction solution was adjusted to 6 by using sodium hydroxide solution (1 mol L⁻¹), a white

precipitate was formed. Then the solution was refluxed for 4 h and filtered immediately. Washed three times with hot alcohol and dried. The terbium complex with ligand L^1 was obtained. The general synthesis procedures of other terbium complexes with ligands L^{2-4} were similar to that of the terbium(III) complex with ligand L^1 .

3 | RESULTS AND DISCUSSION

3.1 | Elemental analysis of the terbium(III) complexes

In order to investigate the elemental contents of the terbium(III) complexes, elemental analysis was conducted, and the molar conductivity was also determined in DMF solution at room temperature. The concentration was 10^{-3} mol L^{-1} . The content of terbium elements in complexes are measured by ethylenediaminetetraacetic acid (EDTA) titrimetric analysis. The data for all the terbium(III) complexes are listed in Table 1.

As shown in Table 1, the composition of the complexes are consistent with the formulas of $Tb(NO_3)_3L^{1-4} \cdot 2H_2O$, since the measured value of elemental contents are in accordance with the theoretical values. The measured molar conductivity values of the terbium(III) complexes in DMF solution are in the range of 65 to 90 $S\ cm^2\ mol^{-1}$, indicating that the terbium(III) complexes are 1:1 electrolytes and a free nitrate ion exists. Therefore, the formulas of the complexes are $[Tb(NO_3)_2L^{1-4}]NO_3 \cdot 2H_2O$.

3.2 | UV analysis

The UV absorption spectra of ligands L^{1-4} and their terbium(III) complexes are recorded in DMF solution. The data are listed in Table 2, and since the UV spectra of all the terbium(III) complexes are similar, only the spectra of L^1 as well as its terbium(III) complex are selected for illustration, as shown in Figure 1.

As seen from Table 2, the absorption bands of ligands L^{1-4} are distributed in the range of 266 to 268 nm and 308 to 326 nm, respectively, and compared to that of the ligands, the maximum absorption peaks of the terbium(III) complexes have red shifts. As shown in Figure 1, $[Tb(NO_3)_2L^1]NO_3 \cdot 2H_2O$ has two peaks at 278 nm and 312 nm, which are due to the $\pi \rightarrow \pi^*$ and $n \rightarrow \pi^*$ transitions, respectively. Compared with the maximum absorption peaks of ligand L^1 (266 nm and 308 nm), that of terbium(III) complex $[Tb(NO_3)_2L^1]NO_3 \cdot 2H_2O$ presents red shifts of 12 nm and 4 nm, respectively. The reason may be that the electron delocalization of the conjugated system of the terbium(III) complexes is increased and the energy required for electron transition is decreased, and it is favorable for the energy

absorption and transition of the complexes. This analysis indicates that the ligands coordinate to the terbium(III) ions successfully.

3.3 | IR spectra analysis

The structure of ligands L^{1-4} and their terbium complexes can be verified by IR spectra. The IR data of the ligands and their terbium(III) complexes are listed in Table 3. Since the IR spectra of all the complexes are similar, only the IR spectra of $[Tb(NO_3)_2L^4]NO_3 \cdot 2H_2O$ as well as its ligand L^4 is selected and shown in Figure 2.

As shown in Table 3 and Figure 2, the complex $[Tb(NO_3)_2L^4]NO_3 \cdot 2H_2O$ exhibits an absorption band at $3459\ cm^{-1}$, this is assigned to the $\nu(O-H)$ stretching vibration and it indicates the existence of water molecules. Compared to the $\nu(C=O)$ stretching vibration absorption peak of ligand L^4 at $1697\ cm^{-1}$, that of the complex $[Tb(NO_3)_2L^4]NO_3 \cdot 2H_2O$ has a red shift of $42\ cm^{-1}$ and a peak located at $1655\ cm^{-1}$. Hence the oxygen atom, of the $C=O$ group coordinated to the terbium(III) ions, has an electron cloud that moves to the terbium ions and thus the bond force constant is changed, so the vibration absorption peak of the carbonyl group exhibits an obvious shift. The $\nu(N-C=O)$ stretching vibration absorption peak also has a red shift from $2361\ cm^{-1}$ to $2356\ cm^{-1}$, this also implied that the oxygen atom of the $N-C=O$ group has coordinated to the terbium(III) ions. The $\nu(C=N)$ stretching vibration absorption peak has a red shift from $1601\ cm^{-1}$ to $1576\ cm^{-1}$, indicating that the nitrogen atom of the $C=N$ group is coordinated to the terbium(III) ions. The complex has characteristic absorption peaks of nitrate groups with a strong absorption peak at $1385\ cm^{-1}$, which showed that the complex has free nitrate groups. Moreover, the symmetric and antisymmetric absorption peaks of the nitrate groups are located at $1340\ cm^{-1}$ and $1458\ cm^{-1}$, and the difference of the vibration frequency ($|v_1 - v_4|$) is less than $200\ cm^{-1}$, indicating that the nitrate groups coordinated to the terbium(III) ions are as bidentate ligands. The earlier mentioned analysis results showed that the ligand L^4 coordinated to the terbium(III) ions successfully, which is consistent with the results of the earlier analysis.

TABLE 2 The UV data of the terbium(III) complexes and corresponding ligands

Complex	λ_{max} (nm)	Ligand	λ_{max} (nm)
$[Tb(NO_3)_2L^1]NO_3 \cdot 2H_2O$	278, 312	L^1	266, 308
$[Tb(NO_3)_2L^2]NO_3 \cdot 2H_2O$	278, 312	L^2	266, 312
$[Tb(NO_3)_2L^3]NO_3 \cdot 2H_2O$	278, 324	L^3	266, 318
$[Tb(NO_3)_2L^4]NO_3 \cdot 2H_2O$	278, 334	L^4	268, 326

TABLE 1 The elemental analysis and molar conductance data of the terbium(III) complexes

Complexes	Measured value (Theoretical value) (%)				Λ_m ($S\ cm^2\ mol^{-1}$)
	Carbon	Hydrogen	Nitrogen	Terbium	
$[Tb(NO_3)_2L^1]NO_3 \cdot 2H_2O$	35.11 (35.01)	3.12 (3.05)	11.03 (11.14)	21.05 (21.08)	65
$[Tb(NO_3)_2L^2]NO_3 \cdot 2H_2O$	33.18 (33.37)	3.01 (2.91)	12.90 (12.98)	21.02 (21.06)	68
$[Tb(NO_3)_2L^3]NO_3 \cdot 2H_2O$	32.12 (32.26)	2.95 (2.82)	11.39 (11.46)	21.39 (21.37)	70
$[Tb(NO_3)_2L^4]NO_3 \cdot 2H_2O$	31.47 (31.58)	2.55 (2.76)	11.14 (11.05)	20.80 (20.92)	72

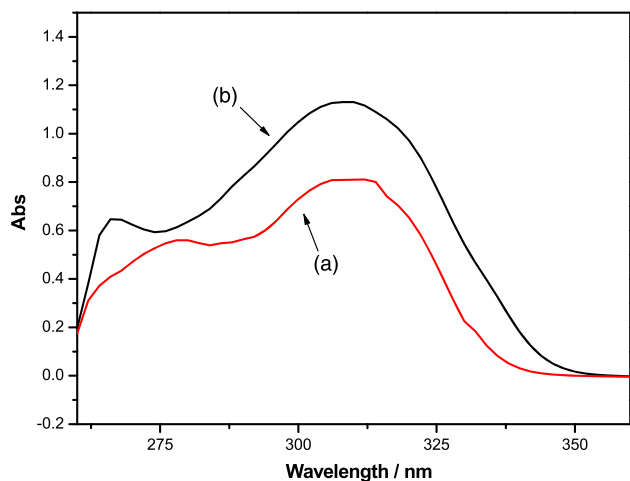


FIGURE 1 The UV spectra of $[\text{Tb}(\text{NO}_3)_2]\text{L}^1\text{NO}_3\cdot 2\text{H}_2\text{O}$ (a) and L^1 (b)

3.4 | Thermal analysis

In order to investigate the thermal stability and decomposition process of the terbium(III) complexes, thermal analysis is carried out under oxygen atmosphere and the data are shown in Table 4. Since the four terbium(III) complexes present similar thermal behaviors, only the thermogravimetric-differential thermal analysis (TG-DTA) curve (Figure 3) of $[\text{Tb}(\text{NO}_3)_2]\text{L}^1\text{NO}_3\cdot 2\text{H}_2\text{O}$ is selected for explanation.

From Table 4 and Figure 3, $[\text{Tb}(\text{NO}_3)_2]\text{L}^1\text{NO}_3\cdot 2\text{H}_2\text{O}$ has a significant endothermic peak at 115°C, and there is a mass loss of 4.56% between 105 and 190°C, that indicated the complex has two crystal water molecules (theoretical contents value of water is 4.78%). Meanwhile, there was a great weight loss of 49.08% between 190 and 470°C, this is consistent with the theoretical contents value (49.53%) of ligand L^1 . Due to the exothermic oxidation of ligand L^1 , there exists an exothermic peak at 393°C. There is a weight loss of 8.73% at 470–570°C, due to the decomposition of the free nitrate ion, and there is also a mass loss of 11.92% between 570 and 650°C, which is assigned to the decomposition of the other two coordinated nitrate ions. This indicated that there was a close connection to whether the nitrate ion is coordinated to the terbium(III) ions or not. Up to 800°C, the complex is completely decomposed and the stable value of the residual is 24.00%, which is consistent with the theoretical value (24.83%) of the rare earth ions oxide (Tb_4O_7). The earlier analysis indicated that the ligand L^1 coordinated with the terbium(III)

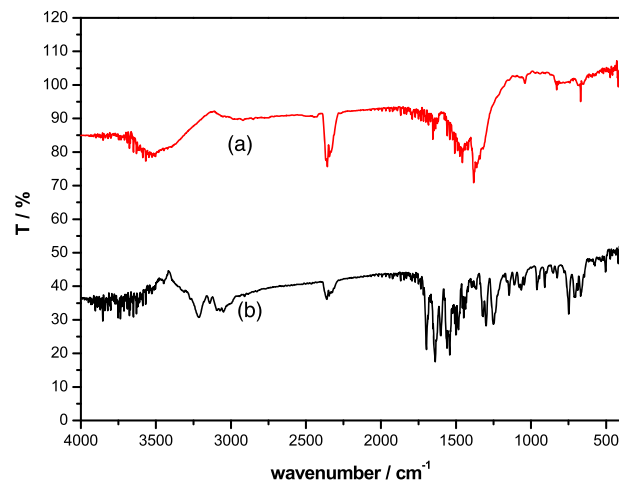


FIGURE 2 The IR spectra of $[\text{Tb}(\text{NO}_3)_2]\text{L}^4\text{NO}_3\cdot 2\text{H}_2\text{O}$ (a) and L^4 (b)

TABLE 4 The thermogravimetric data of the terbium(III) complexes

Complex	Endothermic peak (°C)	Exothermic peak (°C)	Residual weight (theoretical value) (%)
$[\text{Tb}(\text{NO}_3)_2\text{L}^1]\text{NO}_3\cdot 2\text{H}_2\text{O}$	115	393, 600	24.00 (24.83)
$[\text{Tb}(\text{NO}_3)_2\text{L}^2]\text{NO}_3\cdot 2\text{H}_2\text{O}$	113	449, 609	24.14 (24.80)
$[\text{Tb}(\text{NO}_3)_2\text{L}^3]\text{NO}_3\cdot 2\text{H}_2\text{O}$	105	379, 609	25.00 (25.17)
$[\text{Tb}(\text{NO}_3)_2\text{L}^4]\text{NO}_3\cdot 2\text{H}_2\text{O}$	126	401, 615	25.10 (24.97)

ions and the formula of the complex is $[\text{Tb}(\text{NO}_3)_2\text{L}^1]\text{NO}_3\cdot 2\text{H}_2\text{O}$, which is consistent with elemental analysis results. Furthermore, the terbium(III) complex has an endothermic peak at 115°C, which is due to the decomposition of crystal water molecules, this does not change the structure of the terbium(III) complex.^[15] Additionally, it begins to degrade at 190°C, that indicated the terbium(III) complex possesses good thermal stability.^[16]

3.5 | The structure of the ligands and their terbium(III) complexes

According to the results of elemental analysis, UV, IR and thermal analysis, the composition and structure of the terbium(III) complexes can be confirmed. The formulas of the complexes are $[\text{Tb}(\text{NO}_3)_2\text{L}^{1-4}]$

TABLE 3 The IR data of the terbium(III) complexes and corresponding ligands (cm^{-1})

Complex	$\nu(\text{O-H})$	$\nu(\text{C=O})$	$\nu(\text{N-C=O})$	$\nu(\text{C=N})$	$\nu(\text{NO}_3^-)$				
					ν_1	ν_2	ν_3	ν_4	ν
L^1		1693	2351	1599					
$[\text{Tb}(\text{NO}_3)_2\text{L}^1]\text{NO}_3\cdot 2\text{H}_2\text{O}$	3525	1653	2359	1576	1456	1041	835	1340	1385
L^2		1684	2363	1599					
$[\text{Tb}(\text{NO}_3)_2\text{L}^2]\text{NO}_3\cdot 2\text{H}_2\text{O}$	3520	1653	2359	1562	1456	1050	827	1338	1385
L^3		1693	2355	1601					
$[\text{Tb}(\text{NO}_3)_2\text{L}^3]\text{NO}_3\cdot 2\text{H}_2\text{O}$	3523	1647	2372	1577	1458	1059	837	1340	1385
L^4		1697	2361	1601					
$[\text{Tb}(\text{NO}_3)_2\text{L}^4]\text{NO}_3\cdot 2\text{H}_2\text{O}$	3495	1655	2356	1576	1458	1050	830	1340	1385

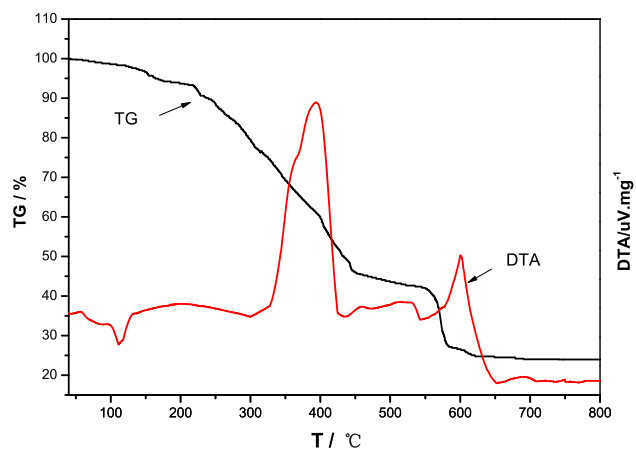


FIGURE 3 The thermogravimetric-differential thermal analysis (TG-DTA) curve of $[\text{Tb}(\text{NO}_3)_2\text{L}^1]\text{NO}_3 \cdot 2\text{H}_2\text{O}$

$\text{NO}_3 \cdot 2\text{H}_2\text{O}$, and the two-dimensional structure of the ligands and their terbium(III) complexes can be deduced and are shown in Figure 4.

3.6 | Fluorescence properties analysis

The excitation spectra of the terbium(III) complexes are determined under the emission wavelength of 545.0 nm, and their fluorescence spectra data are listed in Table 5. Since the spectra of complexes $[\text{Tb}(\text{NO}_3)_2\text{L}^{1-4}]\text{NO}_3 \cdot 2\text{H}_2\text{O}$ are similar, only the spectra (Figure 5) of $[\text{Tb}(\text{NO}_3)_2\text{L}^4]\text{NO}_3 \cdot 2\text{H}_2\text{O}$ is selected for illustration.

It can be seen from Table 5, the four terbium(III) complexes have different fluorescence excitation peaks, located at 275 nm, 278 nm, 276 nm, 281 nm, respectively, and present four characteristic fluorescence emission peaks. As shown in Figure 5, the emission spectrum of complex $[\text{Tb}(\text{NO}_3)_2\text{L}^4]\text{NO}_3 \cdot 2\text{H}_2\text{O}$ consists of four main characteristic

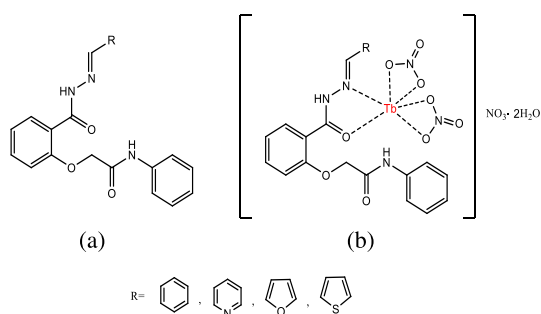


FIGURE 4 The two-dimensional ligands L^{1-4} (a) and their terbium(III) complexes (b)

TABLE 5 Fluorescence spectra data of the terbium(III) complexes

Complexes	λ_{ex} (nm)	${}^5\text{D}_4 \rightarrow {}^7\text{F}_6$		${}^5\text{D}_4 \rightarrow {}^7\text{F}_5$		${}^5\text{D}_4 \rightarrow {}^7\text{F}_4$		${}^5\text{D}_4 \rightarrow {}^7\text{F}_3$	
		λ_{em} (nm)	RLI	λ_{em} (nm)	RLI	λ_{em} (nm)	RLI	λ_{em} (nm)	RLI
$[\text{Tb}(\text{NO}_3)_2\text{L}^1]\text{NO}_3 \cdot 2\text{H}_2\text{O}$	275.0	496.0	383	546.0	1384	583.0	63	622.0	23
$[\text{Tb}(\text{NO}_3)_2\text{L}^2]\text{NO}_3 \cdot 2\text{H}_2\text{O}$	278.0	492.0	377	544.0	1217	585.0	80	621.0	24
$[\text{Tb}(\text{NO}_3)_2\text{L}^3]\text{NO}_3 \cdot 2\text{H}_2\text{O}$	276.0	493.0	154	546.0	848	585.0	26	622.0	11
$[\text{Tb}(\text{NO}_3)_2\text{L}^4]\text{NO}_3 \cdot 2\text{H}_2\text{O}$	281.0	496.0	83	543.0	365	585.0	26	622.0	11

Note: λ_{ex} , exciting wavelength; λ_{em} , emission wavelength; RLI, relative fluorescence intensity.

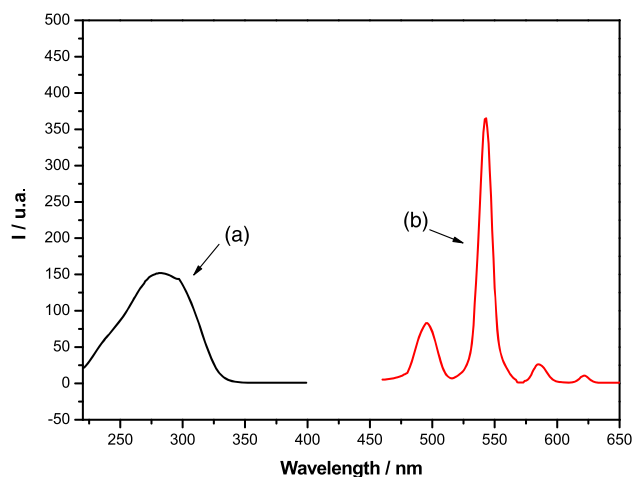


FIGURE 5 The excitation spectrum (a) and emission spectrum (b) of $[\text{Tb}(\text{NO}_3)_2\text{L}^4]\text{NO}_3 \cdot 2\text{H}_2\text{O}$

bands, distributed at 496.0 nm (${}^5\text{D}_4 \rightarrow {}^7\text{F}_6$), 543.0 nm (${}^5\text{D}_4 \rightarrow {}^7\text{F}_5$), 585.0 nm (${}^5\text{D}_4 \rightarrow {}^7\text{F}_4$) and 622.0 nm (${}^5\text{D}_4 \rightarrow {}^7\text{F}_3$). The intensity of the fluorescence emission peaks of the magnetic dipole transition (${}^5\text{D}_4 \rightarrow {}^7\text{F}_6$) and the electric dipole transition (${}^5\text{D}_4 \rightarrow {}^7\text{F}_5$) are stronger than the other two emission peaks, and the emission peak intensity ratio (${}^5\text{D}_4 \rightarrow {}^7\text{F}_5/{}^5\text{D}_4 \rightarrow {}^7\text{F}_6$) is 4.40, indicating that the terbium(III) ion of the complex $[\text{Tb}(\text{NO}_3)_2\text{L}^4]\text{NO}_3 \cdot 2\text{H}_2\text{O}$ is in the asymmetric center. The fluorescence intensity order of the four terbium(III) complexes is $[\text{Tb}(\text{NO}_3)_2\text{L}^1]\text{NO}_3 \cdot 2\text{H}_2\text{O} > [\text{Tb}(\text{NO}_3)_2\text{L}^2]\text{NO}_3 \cdot 2\text{H}_2\text{O} > [\text{Tb}(\text{NO}_3)_2\text{L}^3]\text{NO}_3 \cdot 2\text{H}_2\text{O} > [\text{Tb}(\text{NO}_3)_2\text{L}^4]\text{NO}_3 \cdot 2\text{H}_2\text{O}$. Since the planarity of the benzene ring structure of ligand L^1 is stronger, it can form a better rigid structure with terbium(III) ions; this is suitable to achieve an efficient ligand-to-metal energy transfer, so the terbium ions can be better sensitized and emit characteristic light. This indicated that the fluorescence intensity is determined by the efficiency of the intramolecular energy transfer. The fluorescence emission (antenna effect) is determined by the energy difference between the three excited states (ligand) and the lowest excited state (the central ion), and the emission efficiency is affected by the efficiency of energy transfer. Hence when the ligand absorbs light energy, it transitions from the ground state to the emission state, then the energy is transferred to a triplet state of the ligand by the intersystem crossing, and then intramolecularly transferred to the rare earth ions. Finally, the rare earth ions return back to the ground state from the excited state, and emit characteristic light.^[17,18] Since the energy transferred to the terbium ions is matched better with the energy gap between the ${}^5\text{D}_4 \rightarrow {}^7\text{F}_5$ transition, so the emission peak distributed at 546.0 nm is the highest

among the four peaks. As the terbium(III) complexes with ligand L^1 achieved an efficient ligand-to-metal energy transfer, its fluorescence intensity, therefore, is the strongest among them.

3.7 | Fluorescence quantum yield analysis

Fluorescence quantum yield is measured according to the measure proposed by Yunxiang Ci et al.^[19] The fluorescence quantum yields (Φ_{fx}) are calculated using the following equation:

$$\Phi_{fx} = \frac{n_x^2}{n_{std}^2} \cdot \frac{F_x}{F_{std}} \cdot \frac{A_{std}}{A_x} \cdot \Phi_{std}$$

where n_{std} (1.337) and n_x (1.480) are the refractive index of the solution used for the standard and sample, respectively; the solvent is DMSO; F is the integral area of fluorescence; A is the absorbance in the UV spectrum; $A_{std}/A_x = 1$. The fluorescence quantum yield of the standard solution is 0.55 ($\Phi_{fstd} = 0.55$). The fluorescence quantum yield data of all the terbium(III) complexes are summarized in Table 6.

As shown in Table 6, the order of fluorescence quantum yield of the terbium(III) complexes is as follows: $[Tb(NO_3)_2L^1]NO_3 \cdot 2H_2O > [Tb(NO_3)_2L^2]NO_3 \cdot 2H_2O > [Tb(NO_3)_2L^3]NO_3 \cdot 2H_2O > [Tb(NO_3)_2L^4]NO_3 \cdot 2H_2O$. The fluorescence emission (antenna effect) is determined by the energy difference between the triplet state of the ligand and the lowest excited state of the central ion. Since the rigidity of the benzene ring structure of ligand L^1 is strongest among the ligands, it can form a rigid structure with the terbium ion, so the energy transfer efficiency is the highest among the terbium(III) complexes. Thus, the terbium(III) ion can be better sensitized and its fluorescence quantum yield is the highest. This indicated that the fluorescence quantum yield is related to the planarity of the molecules. Furthermore, the emission efficiency is also affected by the substituent group. Compared to the furan and thiophene, the pyridine ring is an electron deficient heterocyclic compound. Therefore, since the electron-donating group can produce a $p-\pi$ conjugation with the benzene ring and enhance the π conjugation, the fluorescence intensity is enhanced and the fluorescence quantum yield is increased. Hence the fluorescence quantum yield of the complex $[Tb(NO_3)_2L^2]NO_3 \cdot 2H_2O$ is the second highest among them. On the contrary, the electron-withdrawing groups have π electrons and cannot form a conjugation with the benzene ring, and the intersystem crossing is increased, so the fluorescence intensity and the fluorescence quantum yield are decreased. The earlier mentioned results revealed that the introduction of electron-donating groups to the ligand can increase the fluorescence quantum yield of the terbium(III) complexes and the introduction of electron-

withdrawing groups to the ligand can decrease the fluorescence quantum yield of the terbium(III) complexes.

3.8 | Electrochemical properties analysis

The highest occupied molecular orbital (HOMO) energy levels of the terbium(III) complexes are obtained according to the equations $E_{HOMO} = -(4.74 \text{ eV} + E_{Ox})$, where E_{Ox} is the starting value of the oxidation potential peak and is measured with ferrocene as standard. The lowest occupied molecular orbital (LUMO) energy levels of the terbium(III) complexes are calculated by the formula $E_{LUMO} = E_{HOMO} + E_g$, where the energy gap (E_g) is calculated as $E_g = 1240/\lambda_{onset}$ (eV), and λ_{onset} is the value of the largest UV absorption peak.^[20] The electrochemical properties of the terbium(III) complexes are investigated by means of a cyclic voltammetric technique in DMSO solution. The electrochemical data are listed in Table 7, and only the cyclic voltammetry curve of complex $[Tb(NO_3)_2L^1]NO_3 \cdot 2H_2O$ is selected and depicted in Figure 6.

As shown in Table 7 and Figure 6, the order of the oxidation potential (E_{ox}) of the terbium(III) complexes is $[Tb(NO_3)_2L^2]NO_3 \cdot 2H_2O > [Tb(NO_3)_2L^1]NO_3 \cdot 2H_2O > [Tb(NO_3)_2L^4]NO_3 \cdot 2H_2O > [Tb(NO_3)_2L^3]NO_3 \cdot 2H_2O$, the order of the HOMO energy level (E_{HOMO}) is $[Tb(NO_3)_2L^3]NO_3 \cdot 2H_2O > [Tb(NO_3)_2L^4]NO_3 \cdot 2H_2O > [Tb(NO_3)_2L^1]NO_3 \cdot 2H_2O > [Tb(NO_3)_2L^2]NO_3 \cdot 2H_2O$, and the order of the energy gap (E_g) and the LUMO energy level (E_{LUMO}) are $[Tb(NO_3)_2L^1]NO_3 \cdot 2H_2O > [Tb(NO_3)_2L^3]NO_3 \cdot 2H_2O > [Tb(NO_3)_2L^2]NO_3 \cdot 2H_2O > [Tb(NO_3)_2L^4]NO_3 \cdot 2H_2O$. In the pyridine ring, five carbon atoms and one nitrogen atom can provide a single electron p orbital, respectively, and form a conjugated system. However, the electronegativity of the nitrogen atom is larger than that of the carbon, and nitrogen is electron-withdrawing compared to CH. Therefore, the pyridine ring is an electron deficient heterocyclic compound. When ligand L^2 coordinated to terbium ion, the electron cloud density of terbium(III) ion is small and the complex finds it difficult to lose electrons, the oxidation potential is increased and the HOMO energy level is decreased. Since the nitrogen and oxygen atoms of furan and thiophene are in the sp^2 hybrid state, and a five atom or six atom π electron conjugated system can be formed, respectively, they are electron rich aromatic systems. When L^3 or L^4 coordinated to the terbium ion, the electron cloud density of the terbium ion is increased, and the complex easily loses electrons, so the oxidation potential is decreased and the HOMO energy level is increased. Therefore, the oxidation potential of complexes $[Tb(NO_3)_2L^2]NO_3 \cdot 2H_2O$ is the highest and the HOMO energy level is the lowest. This indicated that the oxidation properties, the HOMO energy level and the energy gap of the terbium(III) complexes are

TABLE 6 The fluorescence quantum yields of the terbium(III) complexes

Complex	λ (nm)	I (a.u.)	Φ_{fx}
$[Tb(NO_3)_2L^1]NO_3 \cdot 2H_2O$	316.0	186	0.132
$[Tb(NO_3)_2L^2]NO_3 \cdot 2H_2O$	311.0	157	0.110
$[Tb(NO_3)_2L^3]NO_3 \cdot 2H_2O$	304.0	120	0.084
$[Tb(NO_3)_2L^4]NO_3 \cdot 2H_2O$	313.0	108	0.076

TABLE 7 The electrochemical data of the terbium(III) complexes

Complex	λ_{onset} (nm)	E_{ox} (eV)	E_g (eV)	E_{HOMO} (eV)	E_{LUMO} (eV)
$[Tb(NO_3)_2L^1]NO_3 \cdot 2H_2O$	278	0.581	4.46	-5.321	-0.861
$[Tb(NO_3)_2L^2]NO_3 \cdot 2H_2O$	288	0.591	4.30	-5.331	-1.031
$[Tb(NO_3)_2L^3]NO_3 \cdot 2H_2O$	284	0.564	4.37	-5.304	-0.934
$[Tb(NO_3)_2L^4]NO_3 \cdot 2H_2O$	304	0.574	4.08	-5.314	-1.234

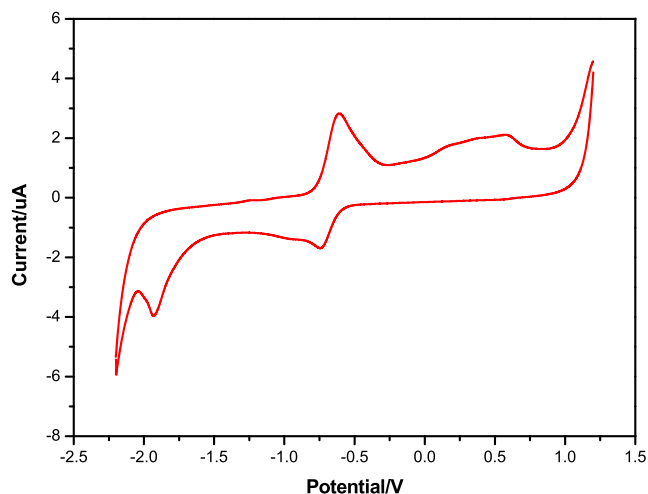


FIGURE 6 The cyclic voltammetry curves of $[\text{Tb}(\text{NO}_3)_2\text{L}^1]\text{NO}_3 \cdot 2\text{H}_2\text{O}$

influenced by the substituent group. From these analyses it can be concluded that the introduction of electron-donating groups to the ligand can enhance the ability to lose electrons, so the oxidation potential is decreased and the HOMO energy level is increased. The introduction of electron-withdrawing groups to the ligand can reduce the HOMO energy levels and increase the oxidation potential of the terbium(III) complexes.

4 | CONCLUSION

Four novel salicyloylhydrazone derivatives were synthesized and characterized by $^1\text{H-NMR}$, $^{13}\text{C-NMR}$ and MS. Their terbium(III) complexes were also prepared, and characterized by molar conductance, elemental analysis, UV spectra, IR spectra and thermal analysis. Furthermore, the formulas of the terbium complexes can be confirmed as $[\text{Tb}(\text{NO}_3)_2\text{L}^{1-4}]\text{NO}_3 \cdot 2\text{H}_2\text{O}$. The thermal analysis results showed that the terbium(III) complexes degraded above 100°C and possessed good thermal stability. The fluorescence properties investigation results showed that the terbium(III) complexes with ligand L^1 possessed the strongest fluorescence intensity, and its fluorescence quantum yield was up to 0.132. The electrochemical analysis results showed that the introduction of electron-donating groups to the ligands can increase HOMO energy levels and decrease the oxidation potential of the terbium(III) complexes. The introduction of electron-withdrawing groups to the ligand can reduce the HOMO energy levels and increase the oxidation potential of the terbium(III) complexes. These results showed that the terbium(III) complexes may possibly be candidates for luminescent material.

ACKNOWLEDGEMENTS

The authors are grateful for the financial support of the National Natural Science Foundation of China (No. J1103312; No.J1210040; No.21341010), the Natural Science Foundation of Hunan Province (No.11JJ5005), Hunan Provincial Science and Technology Department (No.2016SK2064), Changsha Science and Technology Bureau (No. kq1701029; No.kq1701164), the Innovative Research Team in University (No.IRT1238), China Outstanding Engineer Training Plan for Students of Chemical Engineering and Technology in Hunan University (MOE-No.2011-40), and the instrument sharing platform of Hunan University. The authors also thank Dr William Hickey, the US professor of HRM, for the English editing on this article.

ORCID

Dongcai Guo  <https://orcid.org/0000-0001-9975-319X>

REFERENCES

- [1] H. Xin, F. Y. Li, M. Shi, Z. Q. Bian, C. H. Huang, *J. Am. Chem. Soc.* **2003**, *125*, 7166.
- [2] H. Xin, M. Shi, X. C. Gao, Y. Y. Huang, Z. L. Gong, D. B. Nie, H. Cao, Z. Q. Bian, F. Y. Li, C. H. Huang, *J. Phys. Chem. B* **2004**, *108*, 10796.
- [3] R. Cui, W. Liu, L. Zhou, et al., *Dyes Pigm.* **2017**, *136*, 361.
- [4] G. L. Law, K. L. Wong, C. W. Y. Man, W. T. Wong, S. W. Tsao, M. H. W. Lam, P. K. S. Lam, *J. Am. Chem. Soc.* **2008**, *130*, 3714.
- [5] Z. Ye, J. Chen, G. Wang, et al., *Anal. Chem.* **2011**, *83*, 4163.
- [6] L. Wang, J. Tang, N. Sui, X. Yang, L. Zhang, X. Yao, Q. Zhou, H. Xiao, S. Kuang, W. W. Yu, *Anal. Methods* **2017**, *9*, 6254.
- [7] X. Feng, J. Liu, *Inorg. Biochemistry* **2018**, *178*, 1.
- [8] R. K. Sharma, A. V. Mudring, P. Ghosh, *J. Lumin.* **2017**, *189*, 44.
- [9] W. Shan, F. Liu, J. Liu, et al., *J. Inorg. Biochemistry* **2015**, *150*, 100.
- [10] Y. Liu, W. He, Z. Yang, et al., *J. Lumin.* **2015**, *160*, 35.
- [11] W. Zhang, W. He, X. Guo, et al., *J. Alloys Compd.* **2015**, *620*, 383.
- [12] J. Qin, Z. Yang, *Anal. Methods* **2015**, *7*, 2036.
- [13] D. Li, S. Xiong, T. Guo, D. Shu, H. Xiao, G. Li, *Dye. Pigment* **2018**, *158*, 28.
- [14] X. Ni, W. Zhou, Z. Shen, *Chinese J. Catal* **2010**, *31*, 965.
- [15] F. Liao, M. Xu, Q. Liu, J. Li, *National X-ray Diffraction Conference* **2003**, 59.
- [16] C. Guo, L. Zhou, J. Lv, *Polym. Compos* **2013**, *21*, 449.
- [17] T. H. Tran, M. Bentlage, M. M. Lezhnina, U. Kynast, *Photobiol. A Chem* **2014**, *273*, 43.
- [18] M. Latva, H. Takalo, V. M. Mikkala, et al., *J. Lumin.* **1997**, *75*, 149.
- [19] Y. X. Ci, X. Jia, *Chin. J. Anal. Chem.* **1986**, *14*, 616.
- [20] D. Guo, W. He, B. Liu, L. Gou, R. Li, *Luminescence* **2013**, *28*, 280.

How to cite this article: Xiao R, Huang W, Xiao X, Liu Y, Guo D. Novel salicyloylhydrazone derivatives and corresponding terbium(III) complexes: synthesis and properties research. *Luminescence*. 2018;1–8. <https://doi.org/10.1002/bio.3583>